

Reduction of background in optoacoustic image sequences obtained under tissue deformation

Michael Jaeger
Lea Siegenthaler
Michael Kitz
Martin Frenz

University of Bern
Institute of Applied Physics
Sidlerstrasse 5
Bern, 3012
Switzerland

Abstract. For real-time optoacoustic imaging of the human body, a linear array transducer and reflection mode optical irradiation is preferably used. Experimental outcomes however revealed that such a setup results in significant image background, which prevents imaging structures at the ultimate depth limited only by the optical attenuation of the irradiating light and the signal noise level. Various sources of image background, such as bulk tissue absorption, reconstruction artifacts, and backscattered ultrasound, could be identified. To overcome these limitations, we developed a novel method that results in significantly reduced background and increased imaging depth. For this purpose, we acquire, in parallel, a series of optoacoustic and echo-ultrasound images while the tissue sample is gradually deformed by an externally applied force. Optoacoustic signals and background signals are differently affected by the deformation and can thus be distinguished by image processing. This method takes advantage of a combined optoacoustic/echo-ultrasound device and has a strong potential for improving real-time optoacoustic imaging of deep tissue structures. © 2009 Society of Photo-Optical Instrumentation Engineers. [DOI: 10.1117/1.3227038]

Keywords: optoacoustic imaging; photoacoustic imaging; image improvement; background reduction; tumor detection; combined imaging; displacement tracking; elasticity imaging.

Paper 09052PR received Feb. 22, 2009; revised manuscript received Jul. 6, 2009; accepted for publication Jul. 22, 2009; published online Sep. 16, 2009. This paper is a revision of a paper presented at the SPIE conference on Photos Plus Ultrasound: Imaging and Sensing 2009, January 2009, San Jose, California. The paper presented there appears (unrefereed) in SPIE Proceeding Vol. 7177.

1 Introduction

Optoacoustic (OA) imaging is a novel imaging technique with great promise for diagnostics of early cancer, cancer metastasis, and vascular skin diseases.¹⁻⁴ The ultimate imaging depth achievable with OA imaging is determined by the effective optical attenuation coefficient of the tissue and by thermal noise. Strong attenuation of the irradiating light results in low sensitivity for deep tissue structures. The optical penetration depth in, e.g., breast tissue, obtained with near-infrared irradiation, is 1 cm, corresponding to an effective optical attenuation coefficient of 1 cm^{-1} .⁵ The resulting ultimate imaging depth was reported to be as large as 3,^{4,6} 4,⁷ or 5 cm,⁸ or even beyond.⁹ This covers the range where most breast tumors are found.

Although promising results have been achieved in OA imaging of superficial tissue structures both in small animals and humans,^{1-3,10-16} deep OA imaging remains a challenge. The first results of breast cancer imaging *in vivo* were achieved using a transducer array placed in a hemisphere configuration and irradiating perpendicular to the circle plane.^{17,18} This

setup is however strongly specialized for breast imaging, where optical irradiation and acoustic detection on opposite sides of the tissue sample is feasible. For imaging most other parts of the human body, reflection mode OA imaging is generally preferred, where the tissue is irradiated from the same side where OA signals are detected. Reflection mode imaging has the intrinsic advantage of its versatility in imaging different parts of the body using the same device.

Although the ultimate imaging depth does not depend on the mode of irradiation and detection, clinical results of deep OA imaging in reflection mode have not been reported. We have demonstrated that rather than by noise, the imaging depth in reflection mode OA imaging is limited by other, non-stochastic sources of image background. Three main sources of background were identified,^{19,20} namely, optical absorption in the bulk tissue, reconstruction artifacts, and acoustic echoes. In contrast to thermal noise, these sources of background lead to a systematic background, which cannot be reduced by averaging. Only in the case where echo background is caused by a sparse distribution of point-shaped acoustic inhomogeneities can it be iteratively reduced in a regularization approach.²¹ Real human tissue, however, shows a dense structure of acoustic inhomogeneities, which results in speckle patterns well known from echo-ultrasound imaging.

Address all correspondence to: Martin Frenz, University of Bern, Institute of Applied Physics, Sidlerstrasse 5, Bern, 3012, Switzerland. Tel: 41 31 631 89 43; Fax: 41 31 631 37 65; E-mail: frenz@iap.unibe.ch

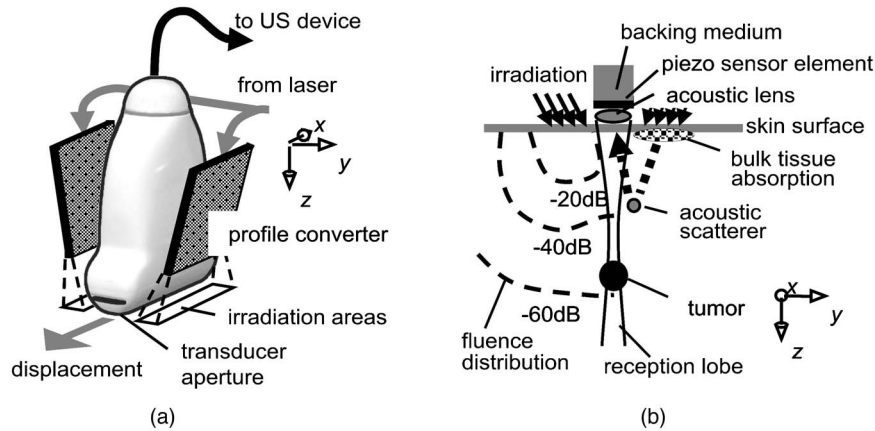


Fig. 1 (a) Setup for OA imaging in reflection mode with a commercial ultrasound array transducer and irradiation optics in a combined transducer head. (b) The transducer shows a narrow reception lobe in elevational direction for imaging of a thin tissue slice, spanned by the transducers axial direction (z) and by the array axis (x). A tumor located deep inside the tissue leads to a weak signal, compared to background signals originating from below the irradiated surface where the laser fluence is high (bulk tissue background). Transients generated at the tissue surface additionally lead to echoes when backscattered by acoustic inhomogeneities (echo background).

In this paper, we theoretically and experimentally investigate a novel optoacoustic detection method that allows one to efficiently reduce echo background, independent on the density of acoustic backscatterers, bulk tissue absorption background, as well as reconstruction artifacts. This method is based on the correlation of optoacoustic images obtained in series from the same tissue sample while the tissue is slightly deformed (e.g., when mechanical stress is exerted using the transducer). The deformation leads to a relative displacement of tissue structures between consecutive OA images. This does affect background and true OA sources differently, thus making it possible for separating them by numerical methods. We propose displacement-compensated averaging (DCA) of consecutive OA images for separating image and background in *real time* and show that using this method image contrast is significantly improved.

2 Theory

We consider the OA imaging setup illustrated in Fig. 1(a). A linear array transducer is acoustically coupled to the surface of the investigated tissue sample. The tissue sample is irradiated through two line profiles, located on either side parallel to the ultrasound transducer array axis. The resulting fluence distribution in the y - z plane shown in Fig. 1(b) is determined by the optical properties of the tissue. The sensitive part of the array transducer is a line of typically 64–128 single pressure sensors parallel to the x -axis. The shape of the pressure sensors, together with a cylindrical acoustic lens placed in front of the array, results in a narrow main lobe of the transducer's elevations angular sensitivity. Therefore, mainly acoustic sources located in a thin tissue slice, spanned by the transducer array axis x and the depth axis z , are imaged.

2.1 Image Background

Three main sources of image background in OA images had been defined.^{19–22}

2.1.1 Bulk tissue background

Bulk tissue background results from irradiating the tissue through surface areas located at a distance d outside the transducer aperture [Fig. 1(b)]. Local spatial fluctuations in the absorption coefficient μ_{abs} of the bulk tissue below the irradiated areas result in OA transients. These transients lead to a significant signal even though the irradiated areas are located outside the imaging plane, where the transducers elevations angular sensitivity is low. The reason is that transients originating within the imaging plane at depth z equal to d , which are detected at the same time with bulk tissue transients, are much weaker due to strong attenuation of light with increasing distance from the irradiated areas. Therefore, if the fluence at depth $z=d$ is small enough compared to the surface fluence, a structure located at that depth within the imaging plane is obscured by the image background originating from the irradiation areas. Figure 2(a) shows bulk tissue background in an experimental OA image of three ink-filled tubes embedded in a pork kidney. The tubes are oriented perpendicular to the imaging plane, thus the cross section of a tube shows up as a dark spot, whereas bulk tissue background appears as a dark “cloud” below 10 mm depth, corresponding to the distance between the array and the irradiation line profiles. The deepest tube is totally obscured by that background.

2.1.2 Echo background

The strong OA transient generated by the high local fluence just below the irradiated area not only propagates straight to the transducer, causing bulk tissue background, but also propagates into the tissue where it gets backscattered from acoustic inhomogeneities [see Fig. 1(b)]. Part of the backscattered transient propagates back into the transducer aperture and generates an echo signal, which can be as strong as an OA signal directly generated by deeply embedded absorbing structures.^{20,21}

Because the acoustic transient causing an echo is generated at the tissue surface, the echo occurs in the OA image as if

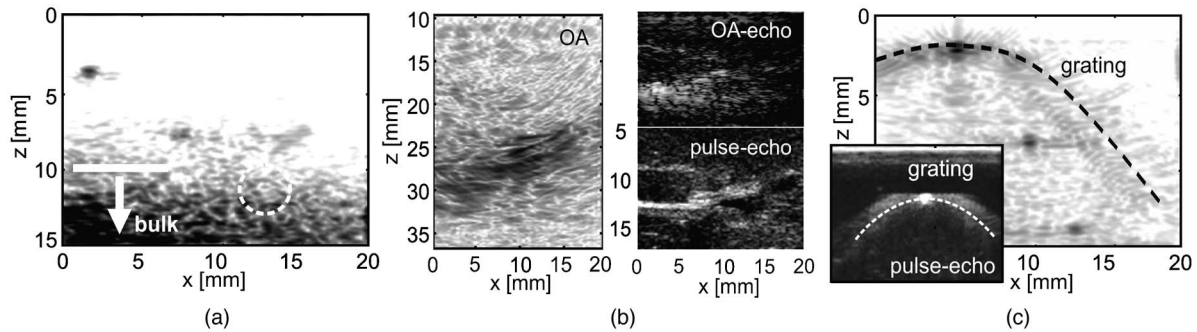


Fig. 2 Sources of background in OA images obtained from a pork kidney. Images were obtained using the setup described in the materials and methods section, and the reconstruction algorithm described in Ref. 23. (a) Bulk tissue absorption leads to significant background in the reconstructed image below 10 mm depth, corresponding to the distance between the irradiated surface area and the array axis. Of the three embedded artificial vessels (dark spots), the deepest one (location indicated by gray circle) is totally obscured. (b) Acoustic transients originating from the surface tissue layer are backscattered and lead to bow-shaped background patterns in the OA image. The nature of echo background becomes obvious if the OA signals are fed into an echo-ultrasound reconstruction algorithm. The resulting image (OA-echo) shows similar features as a true echo image (pulse-echo) acquired at the same location. (c) Grating artifacts show up as bow-shaped “clouds” (indicated by a dashed line) both in OA and echo images.

generated at twice the depth z_{ac} of where the acoustic scatterer is located. Feeding the OA signal data into a reconstruction algorithm designed for pulse-echo imaging, echo background is identified when the resulting image shows features that are also found in a true pulse-echo image. An example of imaging a pork kidney is presented in Fig. 2(b). Strong echo background is caused by the medulla and pelvis. For reconstruction of the echo image from the OA signals (OA-echo), the Fourier algorithm for echo ultrasound imaging described in Ref. 21 was used.

2.1.3 Grating artifact background

Reconstruction artifacts from different OA sources superpose to a quasi random background image. Prominent artifacts result from the grating structure of the array transducer, known in echo ultrasound as grating artifacts [see the inset in Fig. 2(c)]. These artifacts can be disturbing in OA images that show a large dynamic range of the gray level corresponding to the fluence distribution. Grating artifacts spread from the image of a subsurface structure and obscure structures located

deep inside the tissue, which absorb orders of magnitude of less light. Figure 2(c) also shows an OA image of ink-filled tubes embedded in a pork kidney. Because this kidney contained less blood than the one used for Fig. 2(a), bulk tissue background is less pronounced. In addition, the threshold of the image gray level was set to a smaller value in order to accentuate grating artifacts.

2.2 Displacement Compensated Averaging

An externally applied force leads to tissue deformation. OA sources are displaced relative to the imaging transducer. We require a sticky boundary condition at the interface between transducer and tissue surface. Then the relative displacement is spatially dependent, as shown in Fig. 3. We propose a shear deformation of the tissue parallel to the transducer array axis, which leads to a local lateral displacement proportional to the depth z . More generally speaking, the local tissue displacement relative to the transducer is described by a three-dimensional (3-D) vector field $\mathbf{v}(x, y, z) = (v_x, v_y, v_z)$. The tissue deformation is assumed parallel to the x - z plane, such that

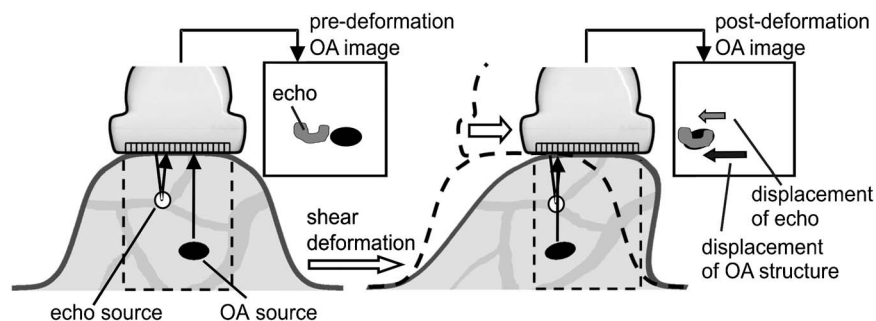


Fig. 3 Sketch showing the relative displacement of tissue structures located at different depths during shear deformation. An absorbing tumor (OA source) located at a certain depth inside a human breast is displaced within the OA image, while the whole breast is deformed applying shear stress to its surface. An acoustic inhomogeneity (echo source) located at half the depth generates an echo of the strong transient originating from the irradiated tissue surface. This echo appears in the OA image as a small cloud at the same depth as the OA source. It is, however, displaced less than the OA source, because the source of the echo is located at half the depth.

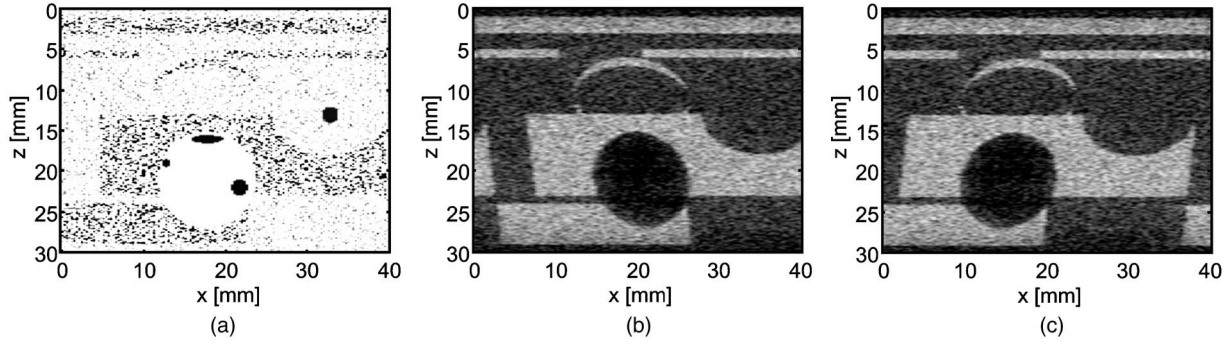


Fig. 4 (a) Digital phantom for testing the DCA method in simulation, including spatially dependent acoustic impedance (gray scale) and OA sources (black). A 2-D cross section of the 3-D phantom, obtained at the location of the imaging plane, is shown. (b) Simulated echo-ultrasound image obtained at surface displacement -3.6 mm and (c) at surface displacement 3.6 mm.

$v_y(x, y=0, z)$ is negligible (i.e., no out-of-plane motion of tissue structures occurs). In a first step, OA images without background are considered. The OA sources visible in the image are all located in the imaging plane ($x, y=0, z$). Because the out-of-plane motion is assumed to be zero, the pre- and postdeformation OA images \mathbf{u} and \mathbf{u}' are related by a linear transformation \mathbf{V}

$$\begin{aligned} \mathbf{u}' &= \mathbf{V}\mathbf{u}, \\ \mathbf{u} &= \mathbf{V}^{-1}\mathbf{u}' = \mathbf{V}^{-1}\mathbf{V}\mathbf{u}. \end{aligned} \quad (1)$$

The transformation operator \mathbf{V} shifts the portion of the image \mathbf{u} at the position (x, z) by the vector $(v_x, v_z)_{x, y=0, z}$ to the new position (x', z') in the image \mathbf{u}' . The second line in eq. (1) states that the predeformation image \mathbf{u} is again obtained if the postdeformation image \mathbf{u}' is compensated for the spatially dependent displacements. \mathbf{V}^{-1} is the transformation, which shifts each point (x', z') in the image back to the corresponding original position (x, z) .

Now image background is considered. The acquired OA image \mathbf{u} can be defined as a superposition of a foreground image assuming no background \mathbf{u}_0 , and the background $\Delta\mathbf{u}$

$$\begin{aligned} \mathbf{u} &= \mathbf{u}_0 + \Delta\mathbf{u}, \\ \mathbf{u}' &= \mathbf{u}'_0 + \Delta\mathbf{u}', \\ \mathbf{u}'_0 &= \mathbf{V}\mathbf{u}_0. \end{aligned} \quad (2)$$

In general, the background is not transformed in the same way as the foreground image. This is explained for the special case where a shear deformation is considered as follows:

1. Echo background: A true OA source, located at position (x, z) in the image plane of the transducer, is displaced by $\mathbf{v}(x, y=0, z)$. An echo reconstructed at the same position (x, z) is displaced by the same amount as the acoustic scatterer from which it emerges. The acoustic scatterer is located at half the depth $z/2$ and therefore displaced only by $\mathbf{v}(x, y=0, z/2)$. If the displacement is proportional to z , then the echo background is displaced by only half the amount of the displacement of the OA source (see Fig. 3).

2. Bulk tissue background: The true depth of the background source (which is located directly below the irradiated surface area) is much smaller than the apparent depth z equal to the distance d between irradiation area and transducer array axis. Therefore, the displacement of bulk tissue background is much smaller than the displacement of OA sources truly located at depth z .

3. Grating artifact background: The grating artifacts spreading out from a pointlike OA source located at depth z_1 are displaced by the same amount as the OA source itself. Therefore, the artifacts are displaced differently than a second OA source located at depth $z_2 > z_1$. Within certain limits (which will be discussed in Sec. 5), it may be assumed that the deformation of the background from $\Delta\mathbf{u}$ to $\Delta\mathbf{u}'$ is described by a linear transformation, similar to the first line in Eq. (1),

$$\Delta\mathbf{u}' = \mathbf{B}\Delta\mathbf{u},$$

$$\Delta\mathbf{u} = \mathbf{B}^{-1}\Delta\mathbf{u}'. \quad (3)$$

If the postdeformation image \mathbf{u}' with background is compensated for the spatially dependent shift as in Eq. (1), then the result is

$$\mathbf{V}^{-1}\mathbf{u}' = \mathbf{V}^{-1}(\mathbf{u}'_0 + \Delta\mathbf{u}') = \mathbf{V}^{-1}(\mathbf{V}\mathbf{u}_0 + \mathbf{B}\Delta\mathbf{u}) = \mathbf{u}_0 + \mathbf{V}^{-1}\mathbf{B}\Delta\mathbf{u}. \quad (4)$$

Because the background is not transformed in the same way as the foreground, $\mathbf{V}_k^{-1}\mathbf{B}_k \neq \mathbf{E}$, where \mathbf{E} is the identity, the displacement of the background is not correctly compensated for. In displacement compensated averaging (DCA), the OA images \mathbf{u}^k obtained after k incremental tissue deformations are all compensated for the displacement \mathbf{V}_k relative to the first image, and then averaged,

$$\begin{aligned}\mathbf{u}_{0,\text{DCA}} &:= \frac{1}{N} \sum_{k=1}^N \mathbf{V}_k^{-1} \mathbf{u}^k = \frac{1}{N} \sum_{k=1}^N \mathbf{V}_k^{-1} (\mathbf{V}_k \mathbf{u}_0 + \mathbf{B}_k \Delta \mathbf{u}) \\ &= \frac{N \mathbf{u}_0}{N} + \frac{1}{N} \sum_{k=1}^N \mathbf{V}_k^{-1} \mathbf{B}_k \Delta \mathbf{u} = \mathbf{u}_0 + O\left(\frac{\sigma_{\Delta \mathbf{u}}}{\sqrt{N}}\right),\end{aligned}\quad (5)$$

where $\sigma_{\Delta \mathbf{u}}^2$ is the local variance of the background image amplitude. Equation (5) states that the standard deviation of the displacement-compensated and averaged background is decreased with increasing number of images N . In the image region, where the difference in the incremental displacement of foreground and background is larger than the width of the background autocorrelation function, the successive displacement-compensated background images are decorrelated. Therefore, the background is reduced inversely proportional to the square root of N . In an experiment, the vector field $(v_x, v_z)_{x,y=0,z}$ can be determined from echo-ultrasound images acquired in parallel with OA images. The displacement of the speckle pattern in the echo images reflects the tissue displacement, which can therefore be estimated using a speckle tracking technique.

Background can be even further reduced if both the foreground transformation \mathbf{V} and the background transformation \mathbf{B} are known. For this purpose, the background $\Delta \mathbf{u}$ itself is reconstructed in a first step, using the DCA method involving the inverse transformation \mathbf{B}^{-1} . The reconstructed background is then subtracted from each image \mathbf{u}^k . In a second step, DCA involving \mathbf{V}^{-1} is applied to the background-adjusted images, yielding an enhanced DCA (EDCA) reconstruction of the foreground image,

$$\begin{aligned}\Delta \mathbf{u}_{\text{DCA}}^k &:= \frac{1}{k} \sum_{l=1}^k \mathbf{B}_l^{-1} \mathbf{u}^l = \dots = \Delta \mathbf{u} + O\left(\frac{\sigma_{\mathbf{u}0}}{\sqrt{k}}\right) \\ \mathbf{u}_{0,\text{EDCA}} &:= \frac{1}{N} \sum_{k=1}^N \mathbf{V}_k^{-1} (\mathbf{u}^k - \mathbf{B}_k \Delta \mathbf{u}_{\text{DCA}}^k) = \dots \\ &= \mathbf{u}_0 + \frac{1}{N} \sum_{k=1}^N \mathbf{V}_k^{-1} \mathbf{B}_k \left(\Delta \mathbf{u} - \Delta \mathbf{u} - O\left(\frac{\sigma_{\mathbf{u}0}}{\sqrt{k}}\right) \right) \\ &= \mathbf{u}_0 + O\left(\frac{\sigma_{\mathbf{u}0}}{\sqrt{N}}\right).\end{aligned}\quad (6)$$

Equation (6) states that using the EDCA method, the original background is fully eliminated in theory. An estimation error of \mathbf{u}_0 is introduced, determined by the local variance $\sigma_{\mathbf{u}0}^2$ of \mathbf{u}_0 . The merit of the EDCA method is that this estimation error is always smaller than the amplitude of the foreground image.

The requirement for the DCA method is the knowledge of the displacement vector field in the imaging plane. For the EDCA method, the displacement vector field of the background is additionally required. This information can be derived from the foreground displacement, knowing the source of background (e.g., in case of echo background, the true depth of echo sources is half the apparent depth in the image). Using this information, the transformation operator \mathbf{B} of the

background can be derived from the transformation operator \mathbf{V} of the foreground image. The limitations of this approach will be discussed in Sec. 5.

3 Materials and Methods

In a first step, we carefully evaluated and compared the DCA and EDCA methods in simulations in which only echo background was taken into consideration. The advantage of simulations as compared to experiments is that the actual local displacement of the tissue is known and the accuracy of the proposed method can be studied independent of the accuracy of the displacement estimation technique. A digital phantom (size $x=40$ mm, $y=60$ mm, $z=30$ mm) included a distribution of local spatial fluctuations of the acoustic impedance and four optically absorbing tumors with different shapes and at different locations. Figure 4(a) shows a 2-D cross section of the tissue phantom at the location of the imaging plane, showing both the acoustic impedance (gray scale) and the OA sources (black). A 128-element linear array transducer was assumed with a tripolar impulse response with 7.5-MHz central frequency, element size 3 mm, and element pitch 0.3 mm. Direct OA, echo-ultrasound and echo background signals were simulated using 3-D Fourier forward algorithms.²⁰ Images were reconstructed using 2-D Fourier backward algorithms.^{21,23} A series of simulated images was obtained with the digital phantom undergoing incremental shear deformation. The transducer and the surface of the digital phantom were moved in steps of 0.6 mm from -3.6 to 3.6 mm parallel to the x -axis, while the bottom of the phantom (at 30 mm depth) was fixed. For the local displacement relative to the transducer, a linear function of depth z was assumed. Figure 4(b) shows the simulated echo-ultrasound image obtained with the transducer positioned at -3.6 mm, and Fig. 4(c) shows the image obtained with the transducer positioned at 3.6 mm. For presentation, both the echo-ultrasound and the OA images were postprocessed for ease of visual interpretation, by envelope detection using Hilbert transformation, by logarithmic compression, and thresholding. For DCA/EDCA, only unprocessed raw OA images were used because the proposed method is based on coherent averaging.

In a second step, a Sigma 5000 IMAGIC medical ultrasound system (Fukuda Denshi Switzerland AG, Basel) was used for the experiments. The software and hardware of the Sigma 5000 was adapted to alternately obtain ultrasound and OA images. A $10 \mu\text{s}$ acquisition time of 64 parallel signal channels, sampled with 40 MHz, could be directly accessed for postprocessing, allowing for reconstruction of an OA image with each single laser pulse. We used a commercial linear array transducer (5-12LA) with central frequency of 7.5 MHz, element size 3 mm, and element pitch 0.3 mm. Given by the limited aperture and acquisition time, only a frame of 20 mm (x direction) by 15 mm (z direction) of the detected tissue slice was accessible for OA imaging. The depth position of this frame was controlled by the trigger delay between laser irradiation and signal acquisition start. For the generation of OA signals, a Q-switched Nd:YAG laser (Coherent, VersaPulse) at $\lambda=1064$ nm was used ($\tau=10$ ns, $E=60$ mJ). The light was guided via a bifurcated fiber bundle with two line converters to irradiate the tissue on two line profiles at either side of the transducer. The minimum irradi-

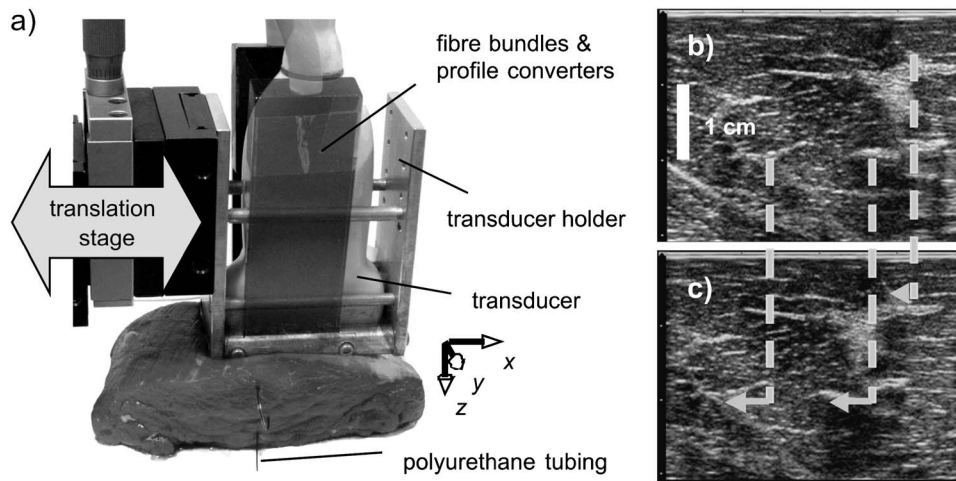


Fig. 5 An OA phantom within the experimental setup. Polyurethane catheter tubing filled with aqueous India ink solution served as blood vessels. (b) Echo image of a phantom obtained at surface displacement -3 mm, and (c) at $+3$ mm.

ated area on the tissue surface was 0.3 cm^2 , resulting in a maximum radiant exposure of 100 mJ/cm^2 . The transducer and the irradiation optics were fixed in a specially designed transducer holder [Fig. 5(a)]. The transducer holder was mounted to a setup including a microcontrolled translation stage for horizontal displacement of the transducer.

Different meat samples were evaluated as bulk tissue material for OA phantoms. Beef was used for the presented example because it contains pronounced echogenic structures and is acoustically transparent [Figs. 5(b) and 5(c)]. The meat sample was cut to a practical size (approximately $10 \times 5 \times 4 \text{ cm}^3$), with the longest dimension perpendicular to the direction of the muscle fibers. During the experiments, the sample together with the transducer was wrapped into a thin plastic foil to avoid desiccation. Polyurethane (PU) catheter tubings (Access Technologies, Illinois) with 0.3 mm i.d. and 0.6 mm o.d. were used as artificial blood vessels [Fig 5(a)]. Three pieces of polyurethane tubing were introduced into the phantom with the aid of a hollow needle with 1 mm i.d. The tubes were filled with 0.5% aqueous solutions India ink (Lefranc & Bourgeois, France). The absorption coefficient of the solution at 1064 nm was determined by transmission spectrometry to $7.9 \pm 0.1 \text{ cm}^{-1}$. The effective optical attenuation coefficient of the meat sample was optoacoustically determined to $2 \pm 0.2 \text{ cm}^{-1}$. For this purpose, a disk-shaped black absorbing layer (radius 1 mm) was painted onto a cover slip and embedded between thin tissue slabs of varying thickness. The OA signal of the black layer was detected in transmission mode using a flat aperture single-element transducer developed in our group.²⁴ This allowed the effective attenuation coefficient to be derived directly from the relation between slab thickness and signal amplitude.

The array transducer was brought into contact to the sample surface via the transducer holder. The orientation of the array axis was chosen perpendicular to the orientation of the muscle fibers in order to provide a speckle pattern with minimum lateral speckle size in the echo-ultrasound images. The sample was slightly compressed to generate sufficient adhesive strength between the sample and transducer. Then, the transducer was horizontally moved in steps of 0.1 mm ,

from a relative horizontal position of -3 to $+3 \text{ mm}$. At each position, a pulse-echo image was acquired. Additionally, at each fifth step, an OA image was acquired. Therefore, in total a number of 13 OA images were acquired, at incremental displacement steps of 0.5 mm .

Although the local displacement vector field was known in the simulations, it had to be estimated in the experiment. For this purpose, the sequence of echo images was fed into a speckle tracking algorithm. The algorithm selected pronounced features in the first image and tracked them throughout the image sequence using correlation maximization. The local displacement was then linearly interpolated from the collection of speckle trajectories.

4 Results

The effect of the DCA method on image contrast of the simulated OA images is illustrated in Fig. 6. In the directly reconstructed images obtained at the different surface displacements, only two OA sources are well recovered [indicated with gray arrows in Figs. 6(a) and 6(b)], while the other two are obscured by background. A comparison of the two images reveals the relative displacement of the visible OA sources in front of the background. All the images were compensated for the displacement relative to the first image and then averaged. This yields the image in Fig. 6(c). DCA leads to horizontal blurring of the background and, therefore, to an increased signal-to-background ratio. In that way, the two OA sources not visible in the direct images are recovered in the averaged image. Application of the EDCA method leads to even further reduction of the background [Fig. 6(d)]. In order to quantitatively compare the contrast improvement obtained by the two methods, the background level was determined as a function of the number of images N used for processing [Figs. 6(e) and 6(f)]. For this purpose, the standard deviation of the image in a region located around the deepest tumor [indicated in Figs. 6(c) and 6(d)] was calculated prior to the postprocessing steps (envelope detection, logarithmic compression, and thresholding).

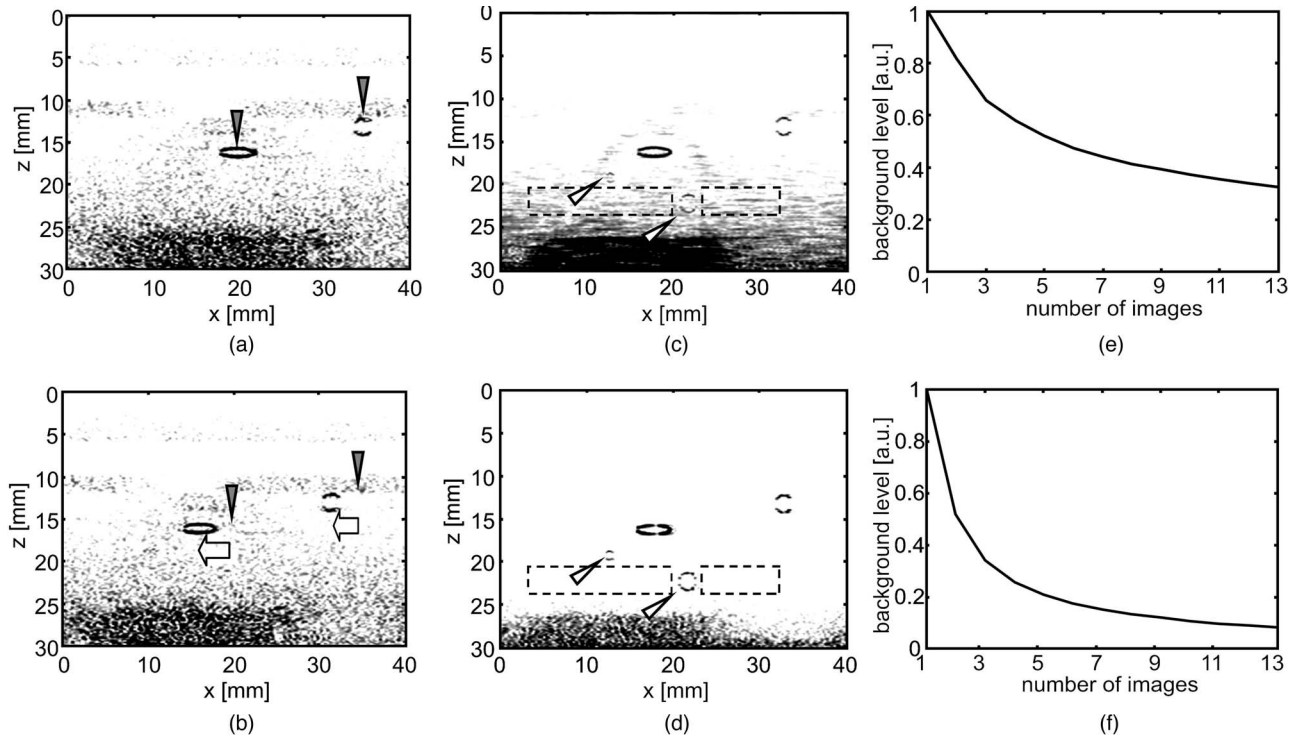


Fig. 6 Effect of the DCA method on image contrast in a simulation: (a) OA images with echo background at surface displacement -3.6 mm and (b) at surface displacement 3.6 mm. Gray arrows indicate constant positions in the two images and illustrate how the visible OA structures are displaced between the two images. (c) Displacement-compensated average of 13 images acquired at surface displacement steps of 0.6 mm. The DCA method leads to an image with increased contrast. Two OA structures initially obscured by echo background are recovered (indicated by white arrows). (d) Using the EDCA method, background is further reduced. (e) Normalized background level as a function of the number of images used for the DCA method. The background level is calculated as the standard deviation of the reconstructed image within the region denoted by dashed rectangles in (c). (f) Normalized background level when using the EDCA method, from the region denoted in (d).

The effect of the DCA method on image contrast of experimental OA images is illustrated in Figs. 7 and 8. In the presented example, three artificial blood vessels were embedded in the meat sample in horizontal configuration at depth $z \approx 24$ mm and $x = 7.5, 12,$ and 14 mm. The positions of the vessels are indicated in the echo-ultrasound image in Fig. 7(a). Figure 7(b) shows the OA image obtained of the same tissue region. In order to decrease stochastic noise and accentuate nonstochastic background, 13 OA images were averaged.

Both the echo-ultrasound and the averaged OA images were acquired at the starting surface displacement position of -3 mm. The vector field of the total local displacements between the first and last position, obtained from echo image speckle tracking, is visualized in Fig. 7(c). The total lateral displacement at the depth of the vessels was -5 mm. Because

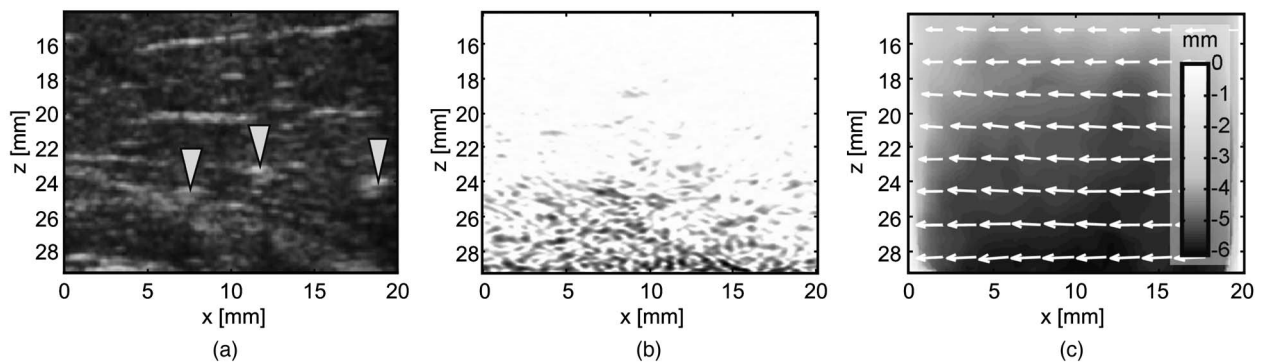


Fig. 7 Experimental data used for testing the DCA method: (a) Echo image of the meat phantom. The positions of the embedded artificial vessels (PU catheter tubes) are indicated by arrows. (b) OA image obtained at a single displacement position, 13 times averaged. (c) Displacement vector field, showing the local displacement between the first (-3 mm) and the last (3 mm) surface displacement position. The vectors are scaled for better visibility.

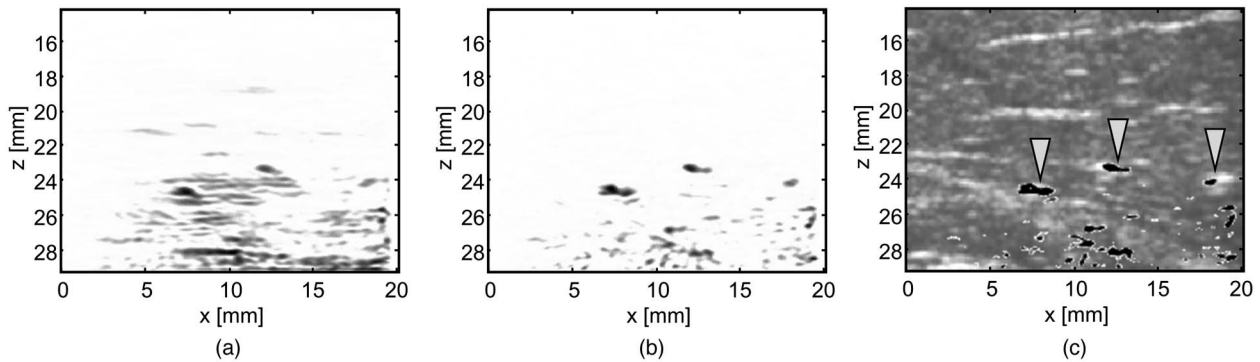


Fig. 8 The DCA method leads to a strongly increased image contrast: (a) Displacement compensated average of 13 consecutive OA images obtained at displacement steps of 0.5 mm. (b) Enhanced DCA of the same images, compensated for the simultaneously reconstructed background. (c) The EDCA image is combined with the echo-ultrasound image. The location of three OA sources clearly coincides with the location of the vessels (indicated by arrows).

the transducer was shifted in positive direction, the local tissue displacement relative to the transducer was negative.

Figure 8(a) shows the DCA image obtained from 13 OA images acquired at 13 different surface displacement positions. In contrast to the image in Fig. 7(b), which was averaged from 13 images acquired at the same position, none of the images used for the DCA was averaged itself. Therefore, the DCA image in Fig. 8(a) results from the same number of direct images as the average image in Fig. 7(b). In comparison to the image obtained at a constant position, the DCA image shows, however, strongly reduced background. This proves that true additional information is introduced by tissue deformation between consecutive images. The DCA method takes advantage of this information. Figure 8(b) shows the image obtained with the EDCA method. EDCA reconstructs in a first step an image of the background. This background image is then subtracted from the OA images, giving an improved estimate of the foreground images already prior to DCA. The experimental result confirms that this procedure results in a much faster increase in contrast compared to applying the DCA directly for reconstruction of the foreground image. The displacement field used for reconstruction of the background is not *a priori* known and therefore determined from the displacement field of the foreground, based on the supposition of the main source of background. In the present example, the supposed main source of background was bulk tissue absorption directly below the irradiated tissue surface ($z=0$), where the displacement is zero. Thus, background was assumed motionless throughout the image sequence. Figure 8(c) shows a combination of the EDCA image with the echo-ultrasound image from Fig. 7(a). The three artificial blood vessels are clearly recovered in the EDCA image.

5 Discussion

Both in simulation and experiment, the DCA method leads to OA images with strongly decreased background and, therefore, increased contrast and imaging depth. The EDCA method has proven the potential of further increasing contrast and imaging depth in agreement with theoretical expectations.

The quantitative analysis based on the simulation suggests that echo background can be reduced by an order of magnitude using EDCA of 13 consecutive OA images. In contrast to

the theoretical expectation [see Eq. (6)], echo background can however not be perfectly reduced using the EDCA method. This may be attributed to following point: The postulated relation between foreground and background displacement was a strong simplification. An acoustic point scatterer located at depth z and reconstructed at depth $2z$ does not show up as a point in the OA image, but as an arc, because the OA reconstruction algorithm leads to a defocused reconstruction of the point scatterer. The whole arc is displaced by the same amount as the point scatterer. When many arcs from scatterers located at slightly different depths intersect, an exact attribution of a displacement to the intersection point is not possible. Yet, if an effective optical attenuation coefficient of 2 cm^{-1} is assumed, the potential increase in imaging depth, corresponding to one order of magnitude background reduction, would be 1.2 cm.

EDCA of the experimental images was also based on a simple relation between the foreground and background displacement. In the case of bulk tissue background, which was assumed the main source of background in the experiment, such a simple relation does however not exist. OA sources reconstructed at position (x, z) in the image can be located anywhere on a circle with radius $r=z$ around the transducer array axis. Bulk tissue signals originate mainly from the region located between the irradiated tissue surface and the penetration depth $z_{\text{eff}}=1/\mu_{\text{eff}}$ of the irradiating light. In the presented experiment, μ_{eff} was $\sim 2 \text{ cm}^{-1}$, corresponding to $z_{\text{eff}}=0.5 \text{ cm}$ penetration depth. Assuming a linear dependence of the displacement from depth z , the displacement of the bulk tissue background can therefore range between 0 and -1 mm (total displacement at 30 mm depth is -6 mm). Therefore, two bulk tissue sources located at the same distance r from the transducer axis are reconstructed at the same depth z , but their individual displacement can vary within a range of 1 mm. The situation with grating artifact background is comparable. Depending on the depth of the source of the artifacts, the background is displaced differently.

The less significant improvement of the experimental result using EDCA as compared to DCA might result from these shortcomings. A more exact formulation of the EDCA method would, in the case of any background layer, include the assumption of multiple background layers. The number of inde-

pendent images needed to fulfill the requirement of additional information would grow with the number of assumed background layers. This might be a limitation to the proposed method when acquiring a large number of images with sufficient tissue strain is difficult.

A further important point influencing, especially, the quality of the experimental outcome of the EDCA method is decorrelation of the OA image background. Speckle patterns in echo-ultrasound images suffer decorrelation upon large tissue deformation. This is an advantage when images obtained from the same tissue structure, but in varying deformation states, are incoherently averaged (strain compounding^{25,26}). Decorrelation of speckle then results in reduced gray-level variance in the averaged image and, therefore, in improved contrast between different tissue types. DCA is related to strain compounding in the sense that images obtained under varying deformation states are compensated for the local displacement and then averaged. However, in contrast to strain compounding, coherent averaging is needed in DCA (i.e., prior to envelope detection and logarithmic compression). Decorrelation of the OA background is even a disadvantage in EDCA because it limits the number of images that can be used for a consistent background reconstruction. Therefore, the potential contrast improvement obtained with EDCA, as compared to DCA, is limited. Fortunately, decorrelation is weak with the shear deformation proposed in this paper, compared to, e.g., axial compression used in elasticity imaging and strain compounding.

It must be mentioned that the quality of the experimental results is also influenced by the fact that only postprocessed (envelope detection, logarithmic compression) echo-ultrasound data were available for speckle tracking. Because the proposed method for background reduction is based on coherent averaging of raw OA images, errors in axial motion estimation can reduce the resulting signal-to-background ratio due to decorrelation of the shift-compensated OA images. Raw radio frequency (RF) beam-former data-based motion tracking as opposed to the envelope-based motion tracking would yield improved accuracy of axial motion estimation.²⁷ Therefore, using RF beam-former echo-ultrasound data instead of envelope data might result in improved images.

In spite of the abovementioned shortcomings, both simulation and experimental results demonstrate that the EDCA method with only one background layer leads to strongly increased image contrast, compared to the simple DCA method. The EDCA method presented in this paper has, moreover, the advantage of very low computational cost compared to any iterative solution of an exactly formulated inverse problem or compared to an EDCA method including multiple background images. The speckle tracking algorithm needed for displacement estimation is a crucial point in real-time application of the presented method. The presented experimental results were obtained with a very simple tracking algorithm. A number of 250 speckles in the echo-ultrasound image was tracked using simple maximum search. The consecutive echo-ultrasound images were acquired at sufficiently small displacement steps such that the displacement of the center of any speckle was always smaller than the speckle size itself. Only small image areas, slightly larger than a speckle, were then used for refining the initial displacement estimation using correlation maximization. Provided sufficiently fine displacement

steps between echo-ultrasound image acquisitions, this approach avoids so-called peak-hopping artifacts without computational overhead and makes the tracking in real time capable.

In a combined echo-ultrasound/OA imaging device, the proposed DCA method might be implemented as follows: The physician conducts the transducer, visually guided by the real-time images. Out of the echo image, he chooses a region of interest using a steerable window, out of which the device extracts a number of speckles. While the examiner moves the transducer slightly back and forth in a free-hand approach, the device tracks these speckles. The displacement vector field is interpolated from the speckle displacement. The frame rate of the echo-ultrasound images would be typically 50 Hz. The frame rate of the OA images is determined by the pulse rate of the Q-switched laser (e.g., 10 Hz). Therefore, five echo-ultrasound images can be acquired in-between consecutive OA images. The portion of the echo-ultrasound and OA image encountered within the chosen window is compensated for the local displacement obtained from the speckle tracking. The resulting image presented to the medical examiner appears motionless. A motionless image has the advantage of ease of interpretation. A disadvantage might be a loss of visual control over the transducer movement. Anyhow, any error in displacement estimation, caused by rapid transducer movement or speckle decorrelation due to out-of-plane motion, would immediately show up as strong distortion in the shift-compensated echo-ultrasound image, which is good feedback for the examiner to reinitialize the procedure. If a moving echo image is preferred for better control of the transducer movement, the OA image might be compensated back for the actual total displacement after DCA processing. In that way, it is always well registered with the echo image. Therefore, the direction of displacement compensation proposed in this paper is not a limiting factor for the DCA method. The relation between foreground and background displacement velocities for the EDCA method might be determined by manually adjusting a sliding bar until the best result is obtained.

Real-time feedback was already found a key element for high contrast-to-noise ratio in elasticity imaging.²⁸ The real-time capability of the presented DCA/EDCA method and the applicability in a free-hand approach gives the medical examiner a visual feedback that guides the evaluation of various modes of transducer movements with direct control of the result. For reducing echo background, shear deformation should yield the best results in theory. A disadvantage of this mode of operation could be the difficulty of keeping a sticky boundary condition between the transducer and skin surface, particularly if ultrasound gel is used for acoustic coupling to the skin. Alternatively, tilting the transducer around the y -axis might yield comparable results. This mode of operation minimizes the shear force exerted on the skin surface, while a linear depth-dependent lateral displacement is maintained. For reduction of bulk tissue background and grating artifacts, vertical tissue compression (i.e., moving the transducer parallel to the depth axis) is an alternative mode of operation. In echo elasticity imaging, axial compression is the preferred way of inducing a spatially dependent tissue displacement because axial displacement can be estimated directly from the unprocessed beam-former RF signal with much higher accuracy than lateral displacement.²⁷ This could also be advantageous for

the DCA method, and information already used for elasticity imaging can readily be incorporated in OA imaging. A disadvantage of this mode of operation for the DCA method might be the comparably small possible total displacement in axial direction and the susceptibility for out-of-plane motion.

6 Conclusion

The experimental results and our simulations revealed that our novel method allows one to strongly increase image contrast in OA images obtained from deep tissue samples in reflection mode. OA images obtained from real tissue in reflection mode are prone to various sources of image background that do not allow to reach the theoretical imaging depth of several centimeters. In the proposed method, information is extracted from deformation of the investigated tissue during combined OA and echo-ultrasound imaging that allows one to differentiate between true OA sources and image background. Because the presented method is computationally inexpensive, it can be implemented in a real-time combined imaging device and shows very promising for OA imaging of large tissue samples, such as the human breast.

Acknowledgments

This research was supported in part by the Swiss National Science Foundation (Grant No. 205320-103872) and the 6th Framework Programme of the European Commission within the Specific Targeted Research Project No. LSHC-CT-2006-018858 PROMET. We specially thank Fukuda Denshi Switzerland for providing us with the echo-ultrasound imaging device and the Ultrasound and Optical Imaging Team of The Institute of Cancer Research, London, for helpful discussions of elasticity imaging techniques.

References

- G. Ku, X. Wang, X. Xie, G. Stoica, and L. V. Wang, "Imaging of tumor angiogenesis in rat brains *in vivo* by photoacoustic tomography," *Appl. Opt.* **44**(5), 770–775 (2005).
- R. I. Siphanto, K. K. Thumma, R. G. M. Kolkman, T. G. van Leeuwen, F. F. M. de Mul, J. W. van Neck, L. N. A. van Adrichem, and W. Steenbergen, "Serial noninvasive photoacoustic imaging of neovascularization in tumor angiogenesis," *Opt. Express* **13**(1), 89–95 (2005).
- K. Maslov, G. Stoica, and L. V. Wang, "In vivo dark-field reflection-mode photoacoustic microscopy," *Opt. Lett.* **30**(6), 625–627 (2005).
- T. D. Khokhlova, I. M. Pelivanov, V. V. Kozhushko, A. N. Zharinov, V. S. Solomatin, and A. A. Karabutov, "Optoacoustic imaging of absorbing objects in a turbid medium: ultimate sensitivity and application to breast cancer diagnostics," *Appl. Opt.* **46**(2), 262–272 (2007).
- T. Durduran, R. Choe, J. P. Culver, L. Zubkov, M. J. Holboke, J. Giammarco, B. Chance, and A. G. Yodh, "Bulk optical properties of healthy female breast tissue," *Phys. Med. Biol.* **47**(16), 2847–2861 (2002).
- S. Manohar, A. Kharine, J. C. G. van Hespren, W. Steenbergen, and T. G. van Leeuwen, "The twente photoacoustic mammoscope: system overview and performance," *Phys. Med. Biol.* **50**(11), 2543–2557 (2005).
- K. H. Song and L. V. Wang, "Deep reflection-mode photoacoustic imaging of biological tissue," *J. Biomed. Opt.* **12**(6), 060503 (2007).
- G. Ku, B. D. Fornage, X. Jin, M. Xu, K. K. Hunt, and L. V. Wang, "Thermoacoustic and photoacoustic tomography of thick biological tissues toward breast imaging," *Technol. Cancer Res. Treat.* **4**(5), 559–565 (2005).
- R. O. Esenaliev, A. A. Karabutov, and A. A. Oraevsky, "Sensitivity of laser opto-acoustic imaging in detection of small deeply embedded tumors," *IEEE J. Sel. Top. Quantum Electron.* **5**(4), 981–988 (1999).
- X. Wang, Y. Pang, G. Ku, G. Stoica, and L. V. Wang, "Three-dimensional laser-induced photoacoustic tomography of mouse brain with the skin and skull intact," *Opt. Lett.* **28**(19), 1739–1741 (2003).
- X. Wang, X. Xie, G. Ku, L. V. Wang, and G. Stoica, "Noninvasive imaging of hemoglobin concentration and oxygenation in the rat brain using high-resolution photoacoustic tomography," *J. Biomed. Opt.* **11**(2), 024015 (2006).
- Y. Wang, X. Xie, X. Wang, G. Ku, K. L. Gill, D. P. O'Neal, G. Stoica, and L. V. Wang, "Photoacoustic tomography of a nanoshell contrast agent in the *in vivo* rat brain," *Nano Lett.* **4**(9), 1689–1692 (2004).
- H. F. Zhang, K. Maslov, M.-L. Li, G. Stoica, and L. V. Wang, "In vivo volumetric imaging of subcutaneous microvasculature by photoacoustic microscopy," *Opt. Express* **14**(20), 9317–9323 (2006).
- M.-L. Li, H. F. Zhang, K. Maslov, G. Stoica, and L. V. Wang, "Improved *in vivo* photoacoustic microscopy based on a virtual-detector concept," *Opt. Lett.* **31**(4), 474–476 (2006).
- L. Z. Xiang, D. Xing, H. M. Gu, D. W. Yang, S. H. Yang, L. M. Zeng, and W. R. Chen, "Real-time optoacoustic monitoring of vascular damage during photodynamic therapy treatment of tumor," *J. Biomed. Opt.* **12**(1), 014001 (2007).
- J.-T. Oh, M.-L. Li, H. F. Zhang, K. Maslov, G. Stoica, and L. V. Wang, "Three-dimensional imaging of skin melanoma *in vivo* by dual-wavelength photoacoustic microscopy," *J. Biomed. Opt.* **11**(3), 34032 (2006).
- S. A. Ermilov, T. Khamapirad, A. Conjusteau, M. H. Leonard, R. Lacewell, K. Mehta, T. Miller, and A. A. Oraevsky, "Laser optoacoustic imaging system for detection of breast cancer," *J. Biomed. Opt.* **14**(2), 024007 (2009).
- S. A. Ermilov, A. Stein, A. Conjusteau, R. Lacewell, T. Miller, S. Thompson, P. Otto, B. McCorvey, T. Khamapirad, M. Leonard, and A. A. Oraevsky, "Detection and noninvasive diagnostics of breast cancer with two-color laser optoacoustic imaging system," *Proc. SPIE* **6437**, 643703 (2007).
- M. Frenz and M. Jaeger, "Optimization of tissue irradiation in optoacoustic imaging using a linear transducer: theory and experiments," *Proc. SPIE* **6856**, 68561Y (2008).
- J. J. Niederhauser, M. Jaeger, and M. Frenz, "Comparison of laser-induced and classical ultrasound," *Proc. SPIE* **4960**, 118–123 (2003).
- M. Jaeger, M. Frenz, and D. Schweizer, "Iterative reconstruction algorithm for reduction of echo background in optoacoustic images," *Proc. SPIE* **6856**, 68561C (2008).
- M. Jaeger and M. Frenz, "Combined ultrasound and photoacoustic system for real-time high contrast imaging using a linear array transducer," in *Photoacoustic Imaging and Spectroscopy*, L. V. Wang, Ed., pp. 289–298, Taylor & Francis Group/CRC, Boca Raton, FL (2008).
- M. Jaeger, S. Schüpbach, A. Gertsch, M. Kitz, and M. Frenz, "Fourier reconstruction in optoacoustic imaging using truncated regularized inverse k-space interpolation," *Inverse Probl.* **23**(6), S51–S63 (2007).
- M. Jaeger, J. J. Niederhauser, M. Hejazi, and M. Frenz, "Diffraction-free acoustic detection for optoacoustic depth profiling of tissue using an optically transparent polyvinylidene fluoride pressure transducer operated in backward and forward mode," *J. Biomed. Opt.* **10**(2), 024035 (2005).
- P. C. Li and M. J. Chen, "Strain compounding: a new approach for speckle reduction," *IEEE Trans. Ultrason. Ferroelectr. Freq. Control* **49**(1), 39–46 (2002).
- P. C. Li and C. L. Wu, "Strain compounding: Spatial resolution and performance on human images," *Ultrasound Med. Biol.* **27**(11), 1535–1541 (2001).
- F. Kallel and J. Ophir, "Three-dimensional tissue motion and its effect on image noise in elastography," *IEEE Trans. Ultrason. Ferroelectr. Freq. Control* **44**(6), 1286–1296 (1997).
- J. C. Bamber and N. L. Bush, "Freehand elasticity imaging using speckle decorrelation rate," in *Acoustical Imaging*, P. Tortoli and L. Masotti, Eds., pp. 285–292, Plenum Press, New York (1996).